

Including real fuel chemistry in LES of turbulent combustion

By A. Felden[†], E. Riber[†], B. Cuenot[†], L. Esclapez, M. Ihme AND H. Wang

Large Eddy Simulation (LES) of an aeronautical burner is performed with two combustion models and a reduced chemical scheme able to accurately describe the combustion of a real multi-component kerosene aviation fuel. The accuracy of the reduced scheme is first assessed on laminar flame cases through comparison with detailed chemistry mechanism. Subsequently, the chemical mechanism is employed in 3D simulations, demonstrating its ability to correctly predict combustion chemistry in turbulent flames.

1. Motivation and objectives

LES is now a widely used tool for the simulation of turbulent combustion in both academic and applied research. At the heart of combustion processes, fuel pyrolysis and oxidation usually proceed through complex and highly non-linear mechanisms involving hundreds of different chemical species. However, the direct integration of such detailed chemistry in LES is not a viable path, because of excessive computational demands and numerical stiffness. It may not be desirable either, as it introduces a large number of reaction parameters, which individually contribute very little to the global flame behavior, yet introducing possibly large uncertainties. In addition, detailed chemistry greatly complicates the modeling and analysis of the strong coupling between turbulence and chemistry.

In practice, combustion simulations use either globally fitted chemical mechanisms (Westbrook & Dryer (1981)), or pre-tabulated laminar flame solutions based on detailed chemistry (Peters (1984) Gicquel *et al.* (2000) Pierce & Moin (2004)). Both methods are able to accurately evaluate global quantities such as flame speed and burnt gas state, but have important, though different, limitations. Global mechanisms severely reduce the number of reaction parameters to less than ten, and are therefore valid only over a narrow range of operating conditions. By construction, they are unable to describe pollutant chemistry or complex, multi-component fuels. On the other hand, pre-tabulated chemistry oversimplifies the interaction between the flame and the flow and cannot easily account for dilution, slow pollutant formation chemistry or heat losses.

As an attempt to find the best compromise between complexity and accuracy in the context of LES, reduced schemes have been introduced (see, e.g., Goussis & Maas (2011)), which accurately describe combustion phenomena by retaining the most important species and reactions in a physically-oriented way. Such schemes, of about ten to 30 species, are nowadays affordable on current high-performance computers, and are non-stiff by construction. The use of such reduced schemes in LES of realistic 3D configurations is still recent and has focused mostly on simple, single-component fuels such as methane or ethylene. Thanks to the recent work by Wang *et al.* (2015) and Gao *et al.* (2015), reduced schemes for real complex fuels are now available and are used in this

[†] CERFACS, France

work to perform LES of an aeronautical combustor operated with kerosene. Two codes are used, AVBP from CERFACS and Vida from CTR and Cascade Inc., to compare two different turbulent combustion models.

First, the derivation and validation of the reduced scheme are presented, and a comparison with a multi-component surrogate fuel model is also provided. Then the 3D configuration chosen to perform the LES is introduced, followed by the validation of the non-reacting flow simulations for the two codes. Finally the results obtained for the turbulent flame are presented and the chemistry accuracy is assessed against experimental data.

2. Real fuel chemistry in LES

Transportation fuels are complex blends of a large number of hydrocarbons. Real fuels are often characterized in terms of chemical features such as average molecular weight (MW), Threshold Sooting Index (TSI), and/or physical features such as density and viscosity (Edwards & Maurice 2001). For practical applications, a real transportation fuel is represented by a surrogate, required to match a set of these characteristic properties as closely as possible. This study focuses on chemical surrogates, meaning that only chemical properties are targeted by the proposed mixture composition.

2.1. *The multicomponent surrogate approach*

Traditionally, real fuel emulation is achieved through the definition of mixtures of one or more selected components, as was the case, for example, in the pioneering work of Wood *et al.* (1989). In the past, the majority of such studies developed surrogates in order to account for the main representative chemical classes thought to be present in the most common real fuels. Recently, Dooley *et al.* (2012) developed a methodology aiming at reproducing the radical pool of a real fuel, through the use of distinct chemical functionalities associated with the potential surrogate components. They proposed a set of four combustion property targets to evaluate the accuracy of such surrogates, namely, the MW, TSI, hydrogen/carbon molar ratio (H/C) and derived cetane number (DCN). Employing a similar technique, but from a numerical point of view and focusing only on individual components that have been previously carefully studied, Narayanaswamy *et al.* (2016) developed an automated tool to derive an optimal surrogate composition. Together with their Component Library Framework, a kinetic mechanism for a multi-component real fuel surrogate is easily obtained. Using these tools together with the combustion property targets of the Jet-A2 fuel POSF10325 reported in Table 1, a detailed kinetic mechanism was derived for a multi-component surrogate *S1* composed of 3 species, the details of which are also reported in Table 1. The associated detailed mechanism is composed of 261 species and 1535 reactions.

2.2. *The HYCHEM methodology*

Another modeling approach has recently been proposed by Wang *et al.* (2015), in which detailed kinetic models for particular real fuels are obtained following a two-step hybrid chemistry (HYCHEM) approach. As a first step, a pyrolysis mechanism consisting of a few lumped reactions yielding primary pyrolysis products is used to describe a single-component surrogate fuel species breakdown. The rates of these pyrolysis reactions are obtained from experimental data of shock tube and flow reactor studies. A detailed kinetic mechanism (USC Mech II here) is then used as a second step to describe the oxidation of the pyrolysis products. The resulting hybrid kinetic models capture shock-tube ignition

Target properties	Jet-A2 POSF10325	Surrogate <i>S1</i>
H/C ratio	1.92	1.91
Average formula	$C_{11.37}H_{21.87}$	$C_{9.48}H_{18.12}$
MW	159	133
Cetane Number	47	47.1
Liquid density [kg/l]	0.8	0.76
Composition [% mole fraction]	18.66% Aromatics 29.45% Total iso-paraffins 20.03% Total n-paraffins 31.86% Total cycloparaffins	37.0% <i>n</i> -dodecane 27.5% iso-octane 35.5% <i>m</i> -xylene

TABLE 1. Combustion property targets (Dooley *et al.* 2012).

delay times and laminar flame speeds over a wide range of pressure, temperature and equivalence ratio (ϕ). The hybrid model for the Jet-A2 POSF10325 fuel (version I), is comprised of 112 species and 790 reactions (amongst which are 6 lumped pyrolysis steps), and the pyrolysis products consist of H_2 , CH_4 , C_2H_4 , C_3H_6 , *i*- C_4H_8 , C_6H_6 and $C_6H_5CH_3$.

2.3. The Analytically Reduced Chemistry (ARC) approach

As discussed in the introduction, solving for all species and reactions present in a detailed kinetic mechanism is currently not feasible in LES. In this work, following the formalism of Tomlin *et al.* (1992), reduced chemistries (ARC) are obtained from detailed kinetic mechanisms following two automated steps. First, a skeletal reduction is performed by identifying redundant species and reactions. Second, the Quasi Steady State (QSS) Approximation is assumed on carefully selected species. The reduction is achieved with the tool YARC of Pepiot (2008), which combines a directed relation graph with error propagation to remove species and reactions and a level of importance criterion to identify QSS candidates.

An ARC is obtained for the Jet-A2 POSF10325 fuel description, the details of which are reported in Table 2. The size of this reduced mechanism allows a direct implementation in the LES solver AVBP, which will be described in Section 3.2. In contrast, reducing the multi-component surrogate *S1* has proven to be much more challenging, due to the competing and interfering pathways of the three components considered. The strong non-linearity of the system eventually prevents us from reducing our original kinetic mechanism to an acceptable size for use in LES. In practice, it is quasi-impossible to fall under 60 species without introducing significant errors on either OH levels or the CO/CO₂ equilibrium. In the following, the detailed mechanism labeled *S1* is employed for comparison in canonical configurations solely.

2.4. Validations

The performances of the ARC based on the hybrid description, named ARC_27_HYCHEM, are evaluated against the detailed mechanism in 0D and 1D canonical test cases with CANTERA (Goodwin *et al.* 2016) and FlameMaster (Pitsch 1996). The results obtained with the detailed *S1* are also included in order to evaluate the effect of the real fuel description. Global quantities targeted by the reduction procedure, such as adiabatic flame temperature, unstrained laminar flame speed and ignition delays are shown to be accurately recovered by the ARC_27_HYCHEM and to be consistent between the two

Transported species										QSS species					
N ₂	H	H ₂	HO ₂	H ₂ O	H ₂ O ₂	O	O ₂	OH	CO	CH ₂	CH ₂ *	C ₂ H ₃	C ₂ H ₅	HCO	HCCO
CO ₂	CH ₃	CH ₄	CH ₂ O	CH ₂ CO	C ₂ H ₂	CH ₂ CHO	CH ₃ O	C ₆ H ₅	C ₆ H ₅ CHO						
C ₂ H ₄	C ₂ H ₆	C ₃ H ₆	C ₅ H ₆	C ₆ H ₆	C ₆ H ₅ O	C ₆ H ₅ CH ₂	A-C ₃ H ₅								
C ₆ H ₄ O ₂	C ₆ H ₅ CH ₃	A-C ₃ H ₄	I-C ₄ H ₈	POSF10325											

TABLE 2. Species contained in the ARC_27_HYCHEM scheme.

fuel models. For concision, these results are not presented here. Note that the S -shaped curves obtained from laminar counterflow diffusion flames, not targeted by the reduction, are similar for all three chemistries with a predicted extinction scalar dissipation rate χ_{ext} value of 52 s^{-1} .

To further characterize the laminar diffusion and premixed flame structures, the evolution across flame fronts of selected species is investigated in Figure 1. These include OH, which is a marker of heat release; CO, which is one of the major pollutants; and C₂H₄, which is the main pyrolysis product of the hybrid chemistry. Premixed flame results include three ϕ while diffusion flame results include a low and a high χ (labelled near equilibrium $\chi = 0.01$ and near extinction $\chi = 47.0$ in Figure 1(a)). The ARC_27_HYCHEM scheme results are found to match the detailed HYCHEM mechanism results on premixed flames but to under estimate the CO mass fraction and over-estimate the C₂H₄ mass fraction on the fuel side of the near equilibrium diffusion flames. These discrepancies are consistent with the reduction targets in terms of equivalence ratio ($0.5 < \phi < 1.5$). The surrogate $S1$ was designed to match the combustion property targets of the Jet-A2 fuel, which are only global quantities. However, a fair agreement is observed between both fuel descriptions on these canonical test cases for most species of interest. Of all the investigated species, C₂H₄ levels exhibit the largest discrepancies on both diffusion and premixed laminar flames: the HYCHEM chemistry always predicts higher levels of C₂H₄. Note that this species is the main pyrolysis product of the HYCHEM approach, when, by contrast, the multi-component approach involves many larger intermediate species. Smaller important species, such as C₂H₂ for instance (not shown), are, however, consistently predicted by both fuel descriptions.

3. Experimental and numerical setup

3.1. Experimental setup

The target configuration is the lean direct injection (LDI) combustor operated at NASA Glenn (Cai *et al.* 2005; Iannetti *et al.* 2008); the experimental configuration is presented in Figure 2(a). Details of the injection system are shown in Figure 2(b). The burner consists of an axial swirler composed of six helicoidal vanes inclined at 60° and a pressure-swirl atomizer located in the center. The atomizer tip is located at the throat of a converging/diverging nozzle. The outer diameter of the nozzle at the combustion chamber dump plane is $D_0 = 0.025 \text{ m}$. The combustion chamber has a height of 305 mm and a square section of length 50.8 mm. Quartz windows allow optical access from all sides.

The combustor is operated at ambient conditions ($P = 1 \text{ atm}$, $T = 300 \text{ K}$). Air is injected with a nominal mass flow rate of 8.16 g/s through a plenum upstream of the swirler vanes while liquid Jet-A2 fuel is injected through the atomizer with a mass flow

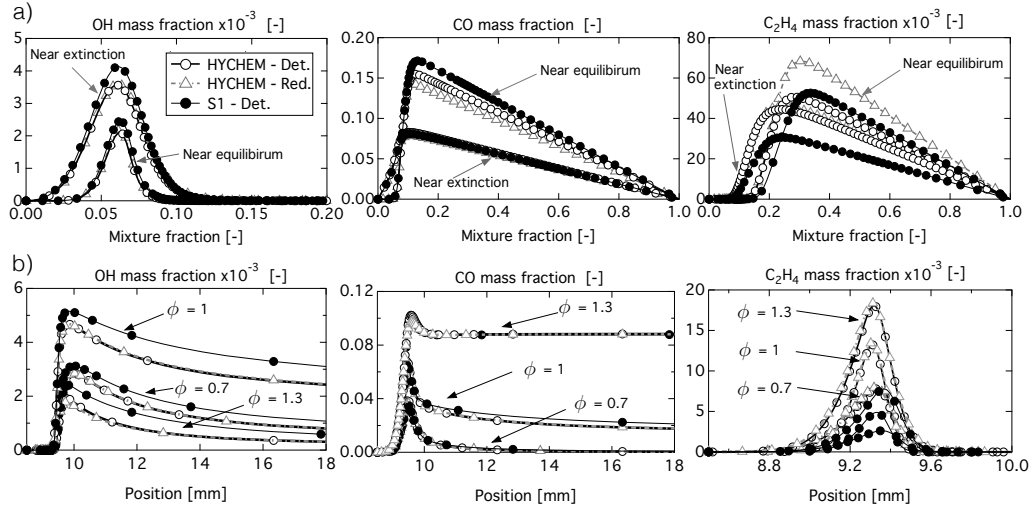


FIGURE 1. OH, CO and C₂H₄ mass fraction profiles. (a) Laminar counterflow diffusion flame at two values of χ . (b) Unstrained laminar premixed flame for three ϕ .

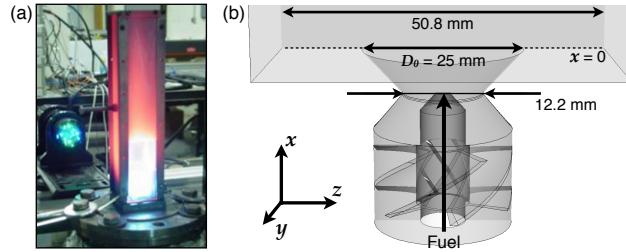


FIGURE 2. (a) Picture of the experimental test rig (Cai *et al.* 2005). (b) Details of the injection system.

rate of 0.415 g/s. These conditions corresponds to a lean overall equivalence ratio ϕ of 0.75. Due to the low pressure in the fuel lines, the spray is found to exhibit unstable distribution patterns (Cai *et al.* 2005). Laser Doppler Velocimetry is used to measure gas velocity while Phase Doppler Particle Analyzer measurements are performed for spray velocity and droplet size distribution (Cai *et al.* 2005). Gas temperature and species profiles are obtained from thermocouple and isokinetic probes, respectively (Iannetti *et al.* 2008).

3.2. Numerical methods

Numerical simulations are performed with two LES solvers: (i) AVBP, a compressible unstructured code developed at CERFACS and IFP-EN (Gicquel *et al.* 2011); (ii) Vida, a low-Mach unstructured solver developed at Cascade Inc. (Ham *et al.* 2007). A comparative overview of the main characteristics of the two numerical set-ups is presented in Table 3.

The computational domain includes the entire test rig, from upstream of the swirler vanes to the downstream end of the combustion chamber. The computational domain is discretized using hexahedral and tetrahedral elements for Vida and AVBP, respectively, keeping approximately the same number of degrees-of-freedom. A Lagrangian approach

	AVBP	Vida
Navier-Stokes formulation	Compressible	Low-Mach
Numerical scheme order (time, space)	$(\mathcal{O}^3, \mathcal{O}^3)$	$(\mathcal{O}^4, \mathcal{O}^4)$
Mesh size (type, nodes)	Hexa, 4 064 672	Tetra, 5 180 244
Walls	No-slip adiabatic	No-slip adiabatic
Spray	Lagrangian	Lagrangian
SGS turb. model	SIGMA	WALE
Combustion model	ARC-DTFLES	Detailed-FPV

TABLE 3. Comparative overview of LES solvers.

is adopted in both LES solvers to describe the spray along with a methodology based on geometric considerations to prescribe pressure-swirl atomizer boundary conditions. The diameter of the injected drops is modeled using a log-normal distribution with a mean of $17 \mu\text{m}$ and a standard deviation of $20 \mu\text{m}$. The drops are injected with a temperature of 300 K. Multi-component evaporation is not considered with the HYCHEM methodology, as we are dealing with a single-component surrogate. The spray cone is set to a mean angle of 70° in order to match the liquid volume flux measurements (Cai *et al.* 2005). The main difference arises from the combustion model: the thickened flame model (DTFLES) (Colin *et al.* 2000) with the ARC_27_HYCHEM scheme is used in AVBP whereas the flamelet/progress variable (FPV) (Pierce & Moin 2004) with the detailed HYCHEM chemistry is used in Vida.

4. Results and perspectives

4.1. Non-reacting flow

For validation purposes, the non-reacting velocity fields obtained from each LES solver are compared against experimental data. Profiles are extracted at three axial positions downstream of the injector tip and are presented in Figure 3. Both LES results are in good agreement with experiments in terms of inner recirculation zone (IRZ) width and velocity magnitude as well as turbulent kinetic energy levels. We note the large opening angle of the swirled jet, which is characteristic of high swirl number flows. Specifically, the swirl number of the injector has a value of 1.0, substantially larger than the critical swirl number of 0.6. The shear layer between the IRZ and the incoming swirled flow exhibits large fluctuations associated with a precessing vortex-core (PVC), also visible from the turbulent kinetic energy profiles of Figure 3(d).

4.2. Reacting flow

The main flow structures are similar to that of the non-reacting case discussed in Section 4.1. The large IRZ extends from just downstream of the pressure-swirl nozzle to about $x = 2 D_0$, and acts as a stabilization mechanism, convecting burnt gases towards the injector tip. Time-averaged velocity profiles at various axial locations are well recovered by both simulations, except in the vicinity of the divergent dump plane, where the radial velocity is underestimated. As discussed by Knudsen *et al.* (2015), the flow-field is only marginally affected by the combustion model. For concision, these results are not presented here.

Figure 4(a) displays time-averaged fields of temperature for both simulations. Isocontours of heat-release rate for AVBP and progress variable source term for Vida dis-

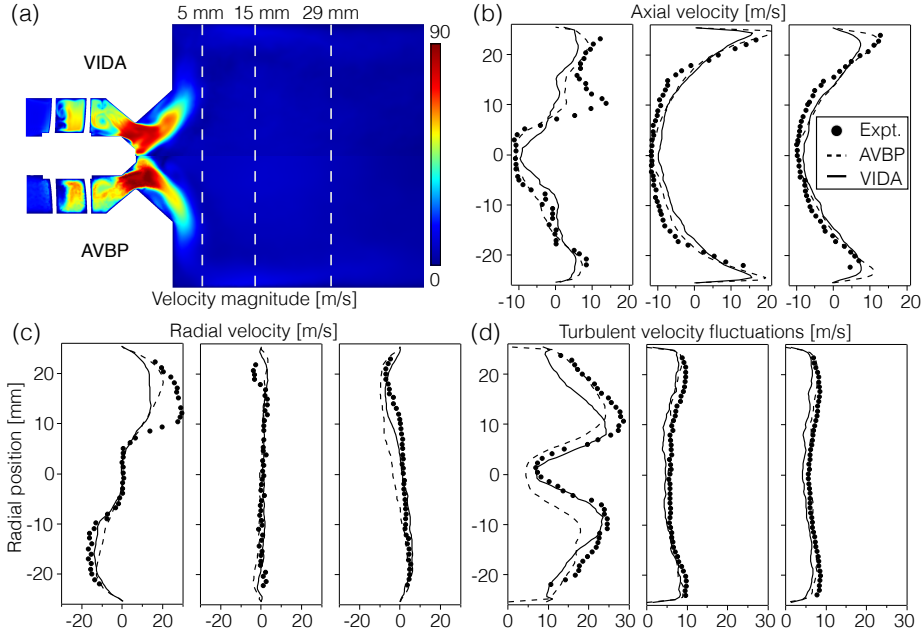


FIGURE 3. (a) Time-averaged fields of velocity magnitude with Vida (top half) and AVBP (bottom half). Time-averaged profiles of (b) axial velocity, (c) radial velocity, and (d) turbulent kinetic energy.

play the flame position, which is found to be sitting closer from the injection system in the case of AVBP. The vertical dashed lines indicate the locations of experimental measurements. In order to investigate the performances of the hybrid approach with both LES, comparisons of time-averaged temperature and species of interest (CO , CO_2 , H_2O) profiles are presented in Figure 4(b,c), for two axial positions located downstream of the dump plane. Main trends are well captured by both LES, although some discrepancies can be observed. Flame regions, identified by the two peaks on the CO profiles at 20 mm, are well captured even though we observe less asymmetry than in the experiments. The temperature of the IRZ is overpredicted by both calculations, especially with the FPV model. A closer examination of the experimental data seems to indicate that the temperature at the outlet of the combustor rig is under the theoretical adiabatic value at the overall ϕ (approximately 300 K below). This difference suggests the presence of heat losses (not included in any simulations) and/or incomplete combustion. Furthermore, droplets' reflection on the walls is frequent in the LES, leading to an increase of fuel availability in the IRZ. This mechanism could be a possible explanation for the overprediction of the temperature and the CO mass fraction in the central zone, at $z = 40$ mm. Ongoing work includes investigation of the sensitivity to the droplet-wall interaction model.

4.3. Effect of combustion model

Instantaneous snapshots of temperature with overlaid droplets calculated with both solvers are provided at the top of Figure 5. As observed in previous studies (Patel & Menon 2008; Knudsen *et al.* 2015), the interaction of the spray with the PVC is crucial to droplet dispersion throughout the combustion chamber. As seen on the snapshots, the

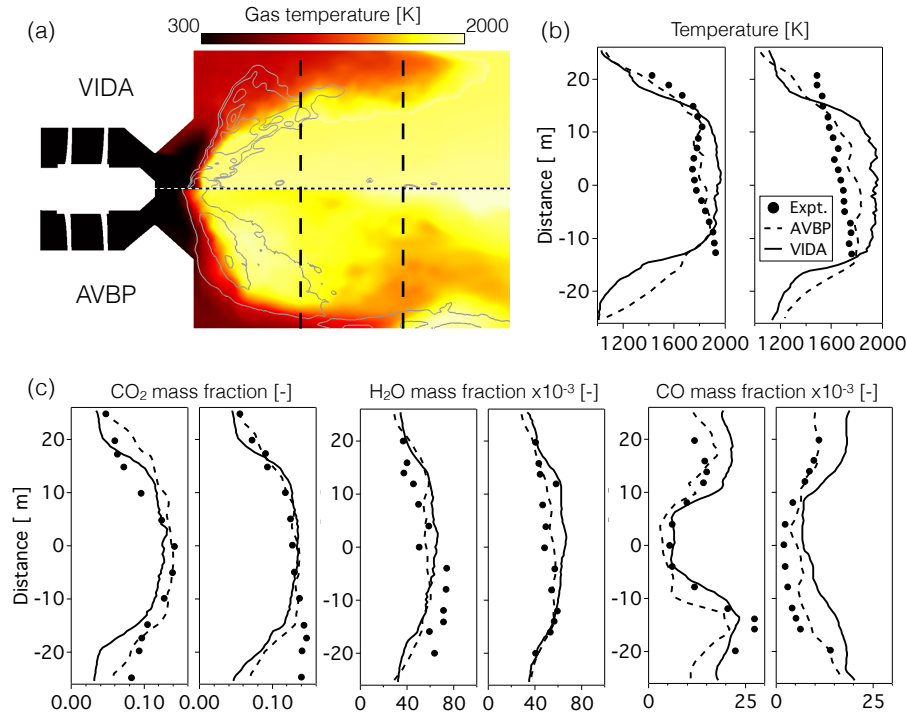


FIGURE 4. (a) Time-averaged temperature field with Vida (top half) and AVBP (bottom half). (b) Temperature profiles at 20 mm and 40 mm downstream of the injector. (c) Species mass fraction profiles at 20 mm and 40 mm.

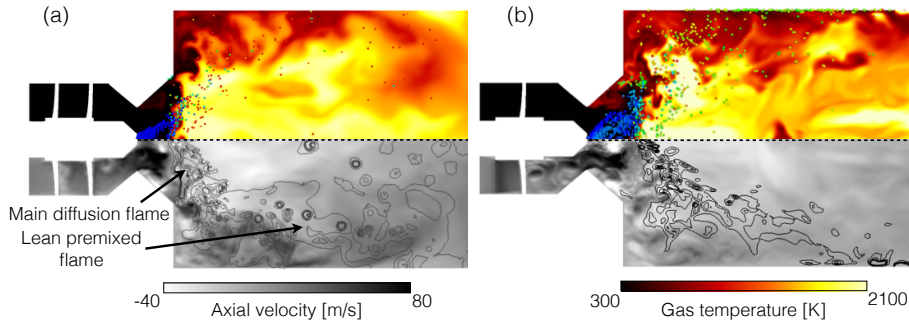


FIGURE 5. Temperature field with droplets (top half) and axial velocity with heat release iso-contours (bottom half) for (a) AVBP and (b) Vida.

spray dynamics exhibit some discrepancies between both LES, and the simulation with Vida appears to undergo a stronger droplet dispersion. This could suggest different PVC topologies, and it is currently under investigation.

The flame structure is rather complex, with a main flame zone directly fed by droplets located in front of the injector, and secondary reaction zones located downstream closer to the combustion walls. The fast evaporation of the small droplets induces strong mixture fraction gradients resulting in diffusion flame structures with intermittent premixed flame pockets in the main flame zone. This diffusion flame is observed in both simulations, even

though the main diffusion flame predicted by Vida is located further downstream. This region extends radially outward along the IRZ and is surrounded by a droplet/air mixture due to droplet dispersion induced by the PVC. As this mixture is convected along the combustion chamber walls, the increasing temperature progressively enables premixing of air and fuel vapor, giving rise to a lean premixed flame front. However, the occurrence and combustion intensity of those premixed fronts are higher in the simulation with AVBP, as can be observed on the snapshots of temperature in Figure 5(top). It is also apparent from the iso-contours of heat release and progress variable source term provided on Figure 4(a) that the premixed flame front is weaker with Vida, which is consistent with the lower mean temperature predicted close to the walls in Figure 4(b). This difference is attributed to the FPV model which is based on diffusion flame structures, so that even though premixed flames can be captured, their heat release rate will surely be lower. Further work should address the question of the tabulated flamelet regime effect in spray combustion. Larger droplets are found to cross both flame fronts and to burn in an isolated droplet regime throughout the combustion chamber, although this behavior could be an artifact of the wall boundary conditions under investigation.

Acknowledgments

The authors would like to thank P. Pepiot from Cornell for fruitful collaboration. This work was performed using HPC resources from GENCI-CCRT (Grant 2015-2b5031), the U.S. DOE under Contract No. DE-AC02-05CH11231 and NASA with award number NNX15AV04A.

REFERENCES

- CAI, J., JENG, S.-M. & TACINA, R. 2005 The structure of a swirl-stabilized reacting spray issued from an axial swirler. In *43rd AIAA Aerospace Sciences Meeting and Exhibit*.
- COLIN, O., DUCROS, F., VEYNANTE, D. & POINSOT, T. 2000 A thickened flame model for large eddy simulations of turbulent premixed combustion. *Phys. Fluids (1994-present)* **12**, 1843–1863.
- DOOLEY, S., WON, S. H., HEYNE, J., FAROUK, T. I., JU, Y., DRYER, F. L., KUMAR, K., HUI, X., SUNG, C.-J., WANG, H. *et al.* 2012 The experimental evaluation of a methodology for surrogate fuel formulation to emulate gas phase combustion kinetic phenomena. *Combust. Flame* **159**, 1444–1466.
- EDWARDS, T. & MAURICE, L. Q. 2001 Surrogate mixtures to represent complex aviation and rocket fuels. *J. Propul. Power* **12**, 461–466.
- GAO, Y., LU, T., XU, R., WANG, H., DAVIDSON, D. F., BOWMAN, C. T. & R. K. HANSON, R. K. 2015 A reduced chemistry model for jet fuel combustion. *Personal communication*.
- GICQUEL, L. Y., GOURDAIN, N., BOUSSUGE, J.-F., DENIAU, H., STAFFELBACH, G., WOLF, P. & POINSOT, T. 2011 High performance parallel computing of flows in complex geometries. *C. R. Mécanique* **339**, 104–124.
- GICQUEL, O., DARABIHA, N. & THÉVENIN, D. 2000 Laminar premixed hydrogen/air counterflow flame simulations using flame prolongation of ILDM with differential diffusion. *Proc. Combust. Inst.* **28**, 1901–1908.
- GOODWIN, D. G., MOFFAT, H. K. & SPETH, R. L. 2016 CANTERA: An object-

- oriented software toolkit for chemical kinetics, thermodynamics, and transport processes. <http://www.cantera.org>, version 2.2.1.
- GOUSSIS, D. & MAAS, U. 2011 Model reduction for combustion chemistry. In *Turbulent Combustion Modeling*, pp. 193–220. Springer.
- HAM, F., MATTSSON, K., IACCARINO, G. & MOIN, P. 2007 Towards time-stable and accurate LES on unstructured grids. In *Complex Effects in Large Eddy Simulations*, pp. 235–249. Springer.
- IANNETTI, A., LIU, N.-S. & DAVOUDZADEH, F. 2008 *The effect of spray initial conditions on heat release and emissions in LDI CFD calculations*. NASA Tech. Report No. NASA/TM—2008-214522 .
- KNUDSEN, E., PITSCH, H. *et al.* 2015 Modeling partially premixed combustion behavior in multiphase LES. *Combust. Flame* **162**, 159–180.
- NARAYANASWAMY, K., PITSCH, H. & PEPIOT, P. 2016 A component library framework for deriving kinetic mechanisms for multi-component fuel surrogates: Application for jet fuel surrogates. *Combust. Flame* **165**, 288–309.
- PATEL, N. & MENON, S. 2008 Simulation of spray–turbulence–flame interactions in a lean direct injection combustor. *Combust. Flame* **153**, 228–257.
- PEPIOT, P. 2008 *Automatic strategies to model transportation fuel surrogates*. PhD Thesis, Stanford University.
- PETERS, N. 1984 Laminar diffusion flamelet models in non-premixed turbulent combustion. *Prog. Energ. Combust.* **10**, 319–339.
- PIERCE, C. D. & MOIN, P. 2004 Progress-variable approach for large-eddy simulation of non-premixed turbulent combustion. *J. Fluid Mech.* **504**, 73–97.
- PITSCH, H. 1996 Flamemaster: a C++ computer program for 0d combustion and 1d laminar flame calculations .
- TOMLIN, A. S., PILLING, M. J., TURÁNYI, T., MERKIN, J. H. & BRINDLEY, J. 1992 Mechanism reduction for the oscillatory oxidation of hydrogen: sensitivity and quasi-steady-state analyses. *Combust. Flame* **91**, 107–130.
- WANG, H., XU, R., HANSON, R. K. & DAVIDSON, D. F. 2015 A Hychem model of jet fuel combustion. *Unpublished*.
- WESTBROOK, C. K. & DRYER, F. L. 1981 Simplified reaction mechanisms for the oxidation of hydrocarbon fuels in flames. *Combust. Sci. and Technol.* **27**, 31–43.
- WOOD, C., MCDONELL, V., SMITH, R. & SAMUELSEN, G. 1989 Development and application of a surrogate distillate fuel. *J. Propul. Power* **5**, 399–405.